Optimal power flow method with consideration of uncertainty sources of renewable energy and demand response

Wenjia Zhang*, Zhuyi Peng, Quanquan Wang, Wanchun Qi and Yi Ge

State Grid Jiangsu Electric Power Co. Ltd. Economic Research Institute, Nanjing, Jiangsu, China

Optimal power flow (OPF) calculation methods are important for the power system operation and mainly focus on the deterministic power flow calculation, neglecting the impact of demand response on online security calculation of power systems with renewable energy sources. Therefore, this paper proposes an OPF calculation method that considers the uncertainties of wind power, photovoltaic (PV) power generation and demand-side response. Firstly, the research focuses on the renewable energy grid, considering the uncertainties of wind power and PV power generation, and establishes uncertainty models for wind power and PV output. Secondly, based on cloud model theory, an uncertainty model for demand response is established. According to the established models, an efficient OPF model is constructed with a linearized submodels considering multiple uncertainties. By testing on the IEEE 30-bus system as a typical example, we found the effectiveness and superiority of the proposed OPF calculation method can benefit the power system economic operation and demand side resource utilization.

KEYWORDS

optimal power flow, demand response, renewable energy grid, cloud model theory, multiple uncertainties

1 Introduction

In recent years, the global energy crisis has become increasingly prominent, and the environmental pollution caused by the combustion of fossil fuels such as coal and oil has also attracted widespread attention (Xin et al., 2022). To address this issue, countries around the world have actively invested a large amount of funds and research personnel in renewable energy technologies to replace fossil fuels. New renewable and clean energy sectors, including wind and solar power generation, have experienced vigorous growth (Chen et al., 2020). As the proportion of wind power, PV and other renewable energy generation in power grid generation continues to increase, the inherent randomness and fluctuation of these energy sources gradually exert a growing impact on the operational state of the electric power system. Therefore, to precisely evaluate how the integration of renewable energy sources with high capacity affects the operational state of the electric power system, and to enhance the reliability and cost-effectiveness of power systems incorporating wind and PV generation, extensive research has been conducted on OPF calculation methods for electric power systems (Yang et al., 2018). Traditional deterministic power flow calculation methods are mainly used in typical scenarios where the grid

structure information of the power system is fixed and the input power at each node of the power system remains basically unchanged. They are unable to accurately reflect the actual operational state of the current power grid where renewable energy sources constitute a significant portion (Pourbehzadi et al., 2019).

Currently, scholars have conducted extensive research on the OPF calculation problem for power grids containing wind power and PVs. In Refs. (Li et al., 2015; Guo et al., 2018), the uncertainty of wind power output is taken into account, and a probabilistic OPF model for wind power integration is proposed. Ref. (Li et al., 2020). introduces a prediction method for PV output that considers correlation and analyzes the OPF of PV output at different time points. Additionally, Ref. (Morshed et al., 2018). addresses the issue of correlation between the outputs of wind farms and proposes a correlation modeling method based on fuzzy C-means clustering for calculating the power flow in a distribution network that includes wind power generation. In Ref. (Yan et al., 2018), Latin Hypercube Sampling (LHS) and its improved algorithm were employed for sampling the probability distributions pertaining to wind power, photovoltaics, and other renewable energy forms, enhancing the speed and accuracy of power flow calculations. In Refs. (Liao et al., 2019; Liu et al., 2019), the linearization semi-variance approach was developed for probabilistic power flow calculations, effectively reducing the impact of uncertainty in clean energy sources like wind power and PVs on power flow calculation results.

However, existing research has not taken into account the impact of demand-side response on OPF calculation. On the load side, demand-side response has a significant influence on the optimal allocation of the power grid. By guiding users' electricity consumption behavior through demand-side response and matching load characteristics with power generation characteristics such as wind power and PVs, it is possible to reduce the configured capacity and optimizes the overall cost-effectiveness of the power grid (Yang et al., 2022). Based on considering the uncertainty of renewable energy generation, Ref. (Zhao et al., 2018). introduced demand-side response, effectively reducing the economic cost of the system. Additionally, due to differences in user demographics, price incentives, and other factors, demand response also exhibits significant uncertainty. Ref. (Lin and Zhang, 2020). considered the impact of demand-side response on system scheduling under different incentive levels, finding that system scheduling costs decrease as incentive levels increase.

In summary, although numerous studies have been conducted on OPF calculation methods for power systems with renewable energy sources, none of them have taken into account the impact of demand-side response on the renewable energy accommodation capacity. As a result, demand-side response has not been incorporated into the OPF calculation methods. Therefore, this paper aims to develop an OPF calculation method that considers the uncertainties of wind power, PV power generation and demand-side response. The decision variables such as the output and terminal voltage of wind turbines, transformer ratio, and reactive power compensation capacity have been reasonably adjusted. This not only reduces the system operating costs while satisfying safety constraints, but also enhancing the speed and accuracy of online security calculation and analysis in power systems.

The remainder of this paper is organized as follows. Section II establishes uncertainty models for wind power and PV output. Section III constructs an uncertainty model for demand-side response. Based on the previously established uncertainty models, and Section IV establishes an OPF model and proposes a linearized method for OPF calculation considering multiple uncertainties. Section V validates the effectiveness and superiority of the proposed method using the IEEE 30-bus system as an example. Finally, Section VI presents the conclusions of this paper.

2 Uncertainty models for wind power and PV output

The fluctuations and intermittency of wind speed and solar irradiance pose new problems and complexities to the stable and economic dispatch of the power grid. This necessitates the use of appropriate mathematical models for accurate calculations of wind power and PV output, facilitating subsequent scenario simulations and uncertainty handling.

2.1 Wind power output model

A wind turbine generator converts wind energy into mechanical energy by driving the rotation of its blades, and then converts this mechanical energy into electrical power. This paper employs the Weibull distribution to fit the measured wind speed data, and the resulting probability density function (PDF) of wind speed is presented as follows in Eq. 1:

$$f(v) = \frac{k}{A}\left(\frac{v}{A}\right)^{k-1} e^{-\left(\frac{v}{A}\right)^k} \tag{1}$$

Where, v represents the actual wind speed (m/s). k and A are the two parameters of the Weibull distribution, which are obtained through fitting the actual data.

The specific mathematical model expression is as follows (Xie et al., 2019) in Eq. 2:

$$P_{wt} = \begin{cases} 0 & v_{out} < v < v_{in} \\ \dfrac{v^3 - v_{in}^3}{v_N^3 - v_{in}^3} P_N & v_{in} \le v \le v_N \\ P_N & v_N < v \le v_{out} \end{cases} \tag{2}$$

Where, P_{wt} is the power of the wind turbine generator. v_{out}, v_{in} and v_N represent the cut-out wind speed, cut-in wind speed and rated wind speed of the wind turbine generator, respectively. P_N is the rated power of the wind turbine generator.

During the operation of a wind turbine generator, only the costs associated with its operation and maintenance are taken into account, and these costs are specifically related to the output power of the turbine. The detailed expression is as follows in Eq. 3:

$$C_{wt}(t) = c_{wt} P_{wt}(t) \tag{3}$$

Where, c_{wt} refers to the cost associated with the routine maintenance and operational expenses of a wind turbine for generating a unit of power. $C_{wt}(t)$ refers to the total cost related

to the routine maintenance and operational expenses of wind turbines during the time period t.

2.2 PV output model

The working principle of PV modules is based on the photoelectric effect, and their power generation is positively correlated with the intensity of light. This paper employs the Beta distribution to fit the measured light intensity data, and the resulting PDF of light intensity is presented as follows in Eq. 4:

$$f(r) = \frac{\Gamma(\alpha + \beta)}{\Gamma(\alpha)\Gamma(\beta)} \left(\frac{r}{r_{\max}}\right)^{\alpha-1} \left(1 - \frac{r}{r_{\max}}\right)^{\beta-1} \quad (4)$$

Where, r represents the light intensity (W/m^2), $r_{\max}$ is the maximum possible light intensity that the photovoltaic power plant can receive, Γ is the Gamma function, which along with parameters α and β, controls the shape of the Beta distribution curve. The values of α and β are obtained through fitting the actual data.

The expression for its output power is as follows (Zhao et al., 2022) in Eq. 5:

$$P_{pv} = rS_{pv}\eta_{pv} \quad (5)$$

Where, P_{pv} signifies the electrical power produced by the PV array. S_{pv} signifies the equivalent area of vertical sunlight received by the photovoltaic cell. η_{pv} represents the photoelectric conversion coefficient.

Similar to wind turbines, only the costs associated with the operation and maintenance of PV cells are considered during their operation. The specific expression is as follows in Eq. 6:

$$C_{pv}(t) = c_{pv}P_{pv}(t) \quad (6)$$

Where, c_{pv} refers to the cost associated with the routine maintenance and operational expenses required for the PV cell to produce a unit of power output. C_{pv} is the total cost related to the routine maintenance and operational expenses incurred by the PV cell during the time period t.

2.3 Simulation of scenarios in wind and solar generation based on monte carlo sampling

When utilizing scenario analysis to tackle the uncertainty inherent in wind and solar generation, it is necessary to first perform scenario simulation to obtain a large-scale scenario sample set. Meanwhile, the method of time series analysis should be employed to consider the coupling characteristics between wind and solar power output at different times. Then, scenario reduction techniques are applied to extract a few typical scenarios from the sample set to describe and characterize the power fluctuations of the entire sample set.

Utilizing Monte Carlo sampling techniques, this paper performs extensive sampling of wind and solar energy production to generate a comprehensive collection of predictive scenarios. Monte Carlo method is based on probabilistic mathematical models and uses numerical simulation
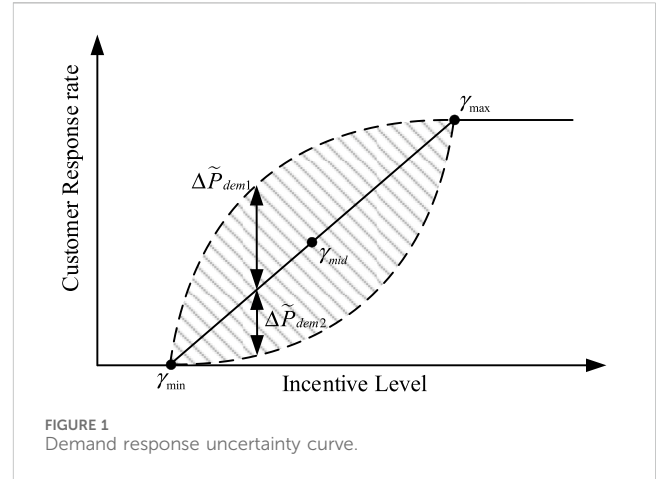

FIGURE 1
Demand response uncertainty curve.

experiments to describe physical geometric characteristics and geometric quantities in order to approximate solutions (Zhao et al., 2023).

For the prediction of wind and solar power output over a scheduling period $T = 24h$, a scenario set of size $N = 1,000$ is obtained through Monte Carlo sampling. The specific description is as follows in Eq. 7:

$$\Omega_S = \left\{S_{wt}^1, S_{wt}^2, S_{wt}^3, ..., S_{wt}^T, S_{pv}^1, S_{pv}^2, S_{pv}^3, ..., S_{pv}^T,\right\} \quad (7)$$

Where, S_{wt}^t represents the set of predicted wind generation scenarios for time t. S_{pv}^t represents the set of predicted PV generation scenarios for the same time t.

Based on the mathematical models established for wind turbines and PV modules in this section, a sample size of $N = 1,000$ and a scheduling period of $T = 24h$ were chosen. The cut-in wind speed is designated as $v_{in} = 2.5m/s$, the cut-out wind speed as $v_{out} = 27m/s$, the rated wind speed as $v_N = 15m/s$. $r = 0.9kW/m^2$. Monte Carlo method was used to obtain 1,000 simulated wind power and photovoltaic output scenarios.

3 Uncertainty model of demand side response

3.1 Controllable load model

The response level of the demand side largely depends on the price compensation strategy issued by the system operator, resulting in significant uncertainty. As shown in Figure 1, when the incentive level is below $\gamma_{\min}$, users generally do not participate in the response. When the incentive level falls between $[\gamma_{\min}, \gamma_{\max}]$, users engage in the response, and the amount of response increases as the incentive level rises. Once the incentive level reaches $\gamma_{\max}$, user response saturates, reaching the maximum response level. It is worth noting that the relationship between user response fluctuations and incentive levels is not linear. As the incentive level increases, the response fluctuations first increase and then decrease. γ_{mid} represents the critical point in the trend of response fluctuation changes.
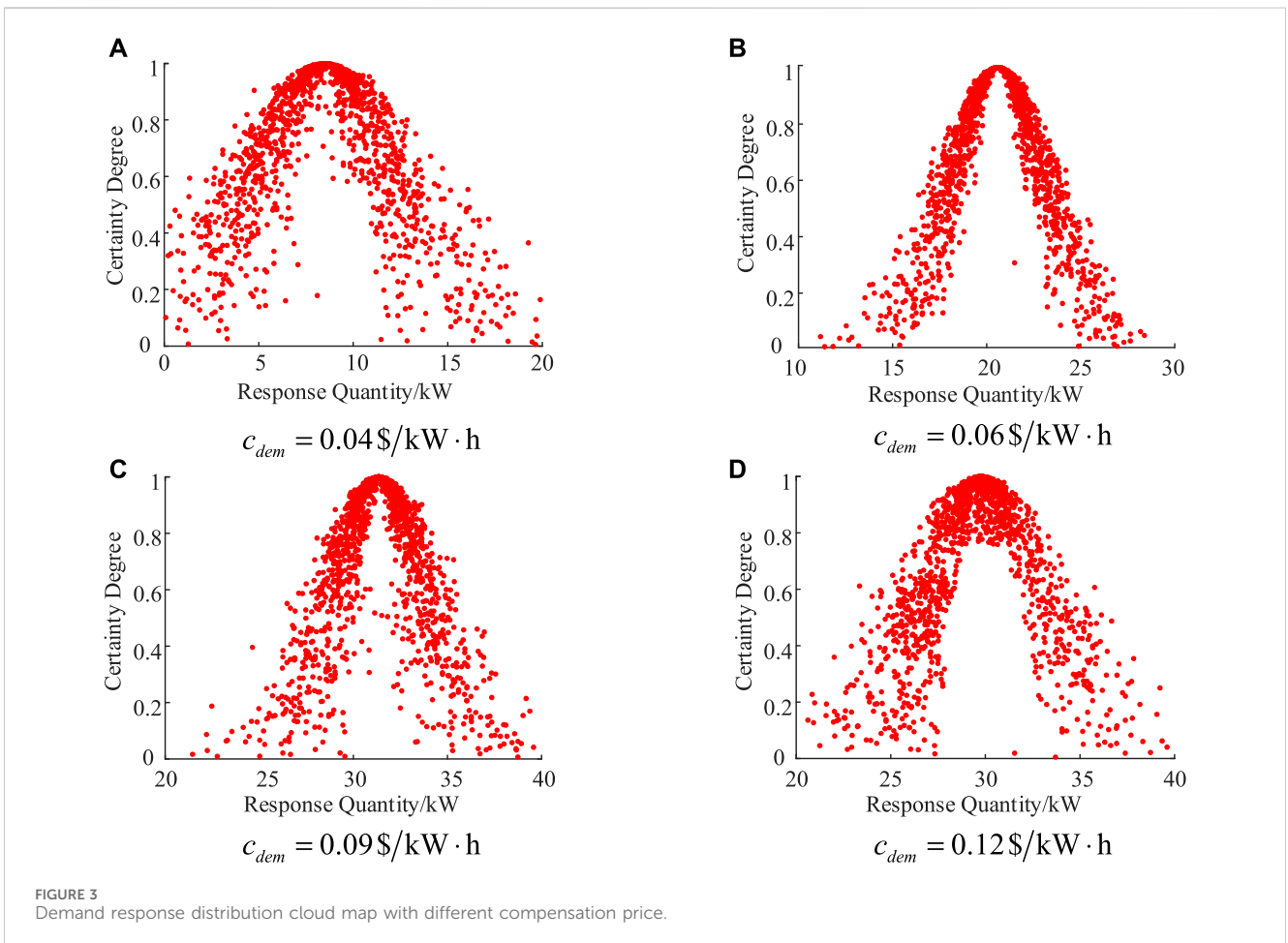
FIGURE 2
Demand response load distribution.
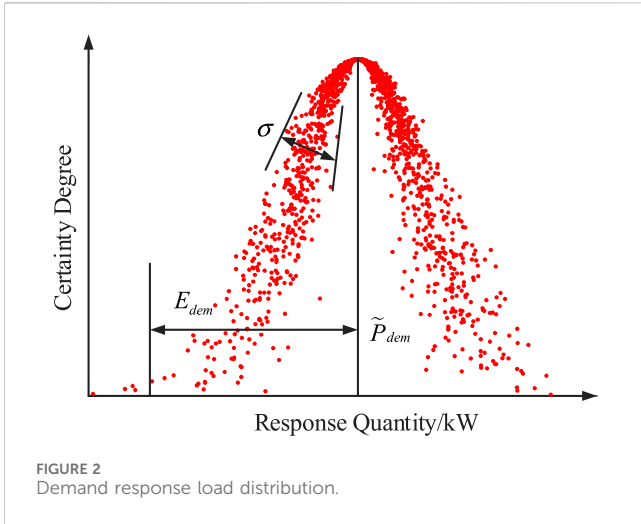
3.2 Establishment of the uncertainty model for demand-side response

In this paper, the theory of cloud model is adopted to describe the uncertainty of demand-side response. Assuming

that the single response quantity P_{dem}^s of a user fluctuates around the expected single response value E_{dem}, the joint effect of n response results from the user forms a user response quantity P_{dem} with an expected response of $\tilde{P}_{dem}$ (Sun et al., 2018). Both P_{dem}^s and P_{dem} follow a normal distribution, and under the condition of $P_{dem}^s = \sigma_s$, the probability density function of P_{dem} is as follows in Eq. 8:

$$f(P_{dem}) = \int_{-\infty}^{+\infty} \frac{1}{\sqrt{2\pi\sigma_s^2}} \exp\left\{-\frac{\left(P_{dem} - \tilde{P}_{dem}\right)^2}{2\sigma_s^2}\right\}$$

$$\cdot \frac{1}{\sqrt{2\pi\sigma^2}} \exp\left\{-\frac{(\sigma - E_{dem})^2}{2\sigma^2}\right\} d\sigma_s \qquad (8)$$

It can be seen that the demand response quantity is a random variable with expected value p_{dem} and variance $E_{dem}^2 + \sigma^2$. When the demand-side compensation price is set at c_{dem}, the cloud distribution of the demand-side load response is illustrated in Figure 2. p_{dem} represents the expected response quantity of users when the compensation price is fixed. E_{dem} characterizes the distribution range of the response quantity, reflecting the degree of uncertainty in the response. σ indicates the concentration of the user response distribution.

FIGURE 3
Demand response distribution cloud map with different compensation price.

3.3 Simulation of demand-side response load scenarios based on the response cloud model

Figure 3 shows the distribution diagram of user responses for 1,000 times under four cases where the compensation price c is 0.04 \$/kW·h, 0.06 \$/kW·h, 0.09 \$/kW·h and 0.12 \$/kW·h respectively.

4 OPF model and solution

4.1 Establishment of the OPF model

To perform OPF calculations, the initial step involves establishing an OPF model. This paper proposes an OPF model that comprehensively incorporates multiple uncertainties, primarily the fluctuations in wind turbine output and PV generation, along with the uncertainty associated with demand-side response. The specific composition of the OPF model includes: the objective function, the equality constraints for power balance, and a set of inequality constraints (Sun et al., 2018).

4.1.1 Objective function

$$f = \min\left[\sum_{i=1}^{m}\left(a_i + b_i P_{Gi} + c_i P_{Gi}^2\right) + C_{comp}\right] \quad (9)$$

$$C_{comp} = c_{dem}P_{dem} \quad (10)$$

Where, the objective function f is composed of two parts in Eqs 9 and 10: the system's generation expenses and the compensation expenses for user load shedding, excluding expenses such as unit outages. a_i, b_i and c_i represent the generation cost factors within the power grid. P_{Gi} represents the active power outputted by the generator situated at node i. m denotes the quantity of generator nodes present within the power grid. C_{comp} represent the compensation expenses for user load shedding.

4.1.2 Equality constraints

The equality constraints primarily consist of the nodal power flow balance constraints in Eq. 11:

$$\begin{cases} P_{Gi} + P_{wt}^i + P_{pv}^i - P_{load}^i - P_{node}^i = 0 \\ Q_{Gi} + Q_{wt}^i + Q_{pv}^i - Q_{load}^i - Q_{node}^i = 0 \end{cases} \quad (11)$$

Where, Q_{Gi} represents the reactive power generated by the generator at node i. P_{node}^i and Q_{node}^i are the active and reactive power injection at node i, respectively. P_{lode}^i and Q_{lode}^i are the active power and reactive power flowing into node i, respectively.

4.1.3 Inequality constraints

$$\begin{cases} P_{Gi}^{\min} \le P_{Gi} \le P_{Gi}^{\max} \\ Q_{Gi}^{\min} \le Q_{Gi} \le Q_{Gi}^{\max} \\ U_i^{\min} \le U_i \le U_i^{\max} \\ P_{nodei}^{\min} \le P_{node}^i \le P_{nodei}^{\max} \\ Q_{nodei}^{\min} \le Q_{node}^i \le Q_{nodei}^{\max} \end{cases} \quad (12)$$

In Eq. 12, where, U_i denotes the voltage magnitude at node i. $P_{Gi}^{\max}$, $P_{Gi}^{\min}$, $Q_{Gi}^{\max}$ and $Q_{Gi}^{\min}$ represent the upper and lower limits of the active power output and the upper and lower limits of the reactive power output of the generator at node i, respectively. $U_i^{\max}$ and $U_i^{\min}$ represent the upper and lower limits of the voltage at node i, respectively. $P_{nodei}^{\max}$, $P_{nodei}^{\min}$, $Q_{nodei}^{\max}$ and $Q_{nodei}^{\min}$ represent the upper and lower limits of active power and the lower and upper limits of reactive power carried by node i, respectively (Li et al., 2023).

4.2 Solution of OPF model

The nonlinearity of the OPF model considering multiple uncertainties is primarily concentrated in the equality constraints of the nodal power balance equations and the line active power flow equations. This paper introduces a linearization approach for OPF calculations, incorporating uncertainties in wind and solar energy generation, along with demand-side response considerations, through simplified approximations of the node power balance equations.

The power inflow at node i is expressed as follows:

$$\begin{cases} P_{node}^i = \sum_{j=1}^{n} G_{ij}U_iU_j \cos\theta_{ij} + \sum_{j=1}^{n} B_{ij}U_iU_j \sin\theta_{ij} \\ Q_{node}^i = \sum_{j=1}^{n} G_{ij}U_iU_j \sin\theta_{ij} - \sum_{j=1}^{n} B_{ij}U_iU_j \cos\theta_{ij} \end{cases} \quad (13)$$

Where, G_{ij} and B_{ij} are respectively the real part and the imaginary part of the element in the ith row and jth column of the node admittance matrix. θ_{ij} is the voltage phase angle difference between node i and node j.

The node admittance matrix of a power system exhibits a unique structure, where the diagonal elements are the sums of the admittances of the non-diagonal elements as well as the shunt components connected to each node.

$$Y_{ij} = \begin{cases} -y_{ij} & i \ne j \\ y_{ii} + \sum_{k=1,k \ne i}^{n} y_{ik} & i = j \end{cases} \quad (14)$$

Where, Y_{ij} is the node admittance matrix element of line i-j. y_{ij} is the admittance of line i-j. y_{ii} is the self-admittance of node i. Based on this, Eq. 13 is reformulated.

$$P_{node}^i = \sum_{j=1}^{n} G_{ij}U_iU_j \cos\theta_{ij} + \sum_{j=1}^{n} B_{ij}U_iU_j \sin\theta_{ij}$$
$$= g_{ii}U_i^2 + \sum_{j=1,j \ne i}^{n}\left[g_{ij}U_i\left(U_i - U_j \cos\theta_{ij}\right) - b_{ij}U_iU_j \sin\theta_{ij}\right] \quad (15)$$

Where, g_{ij} and b_{ij} are the conductance and susceptance of line i-j, respectively. An expression can be derived from mathematical approximation formulas as follows in Eq. 16:

$$U_i\left(U_i - U_j \cos\theta_{ij}\right) \approx U_i\left(U_i - U_j\right)$$
$$= (1 + \Delta U_i)\left(\Delta U_i - \Delta U_j\right) \approx \left(\Delta U_i - \Delta U_j\right)$$
$$= \left[1 + \Delta U_i - \left(1 + \Delta U_j\right)\right] = U_i - U_j \quad (16)$$

TABLE 1 Basic parameter table.

	Scenario 1	Scenario 2	Scenario 3	Scenario 4
c_{dem}(\$/kW·h)	0.04	0.06	0.09	0.12
Probability	0.216	0.175	0.308	0.301

Wind power output scenario

PV output scenario

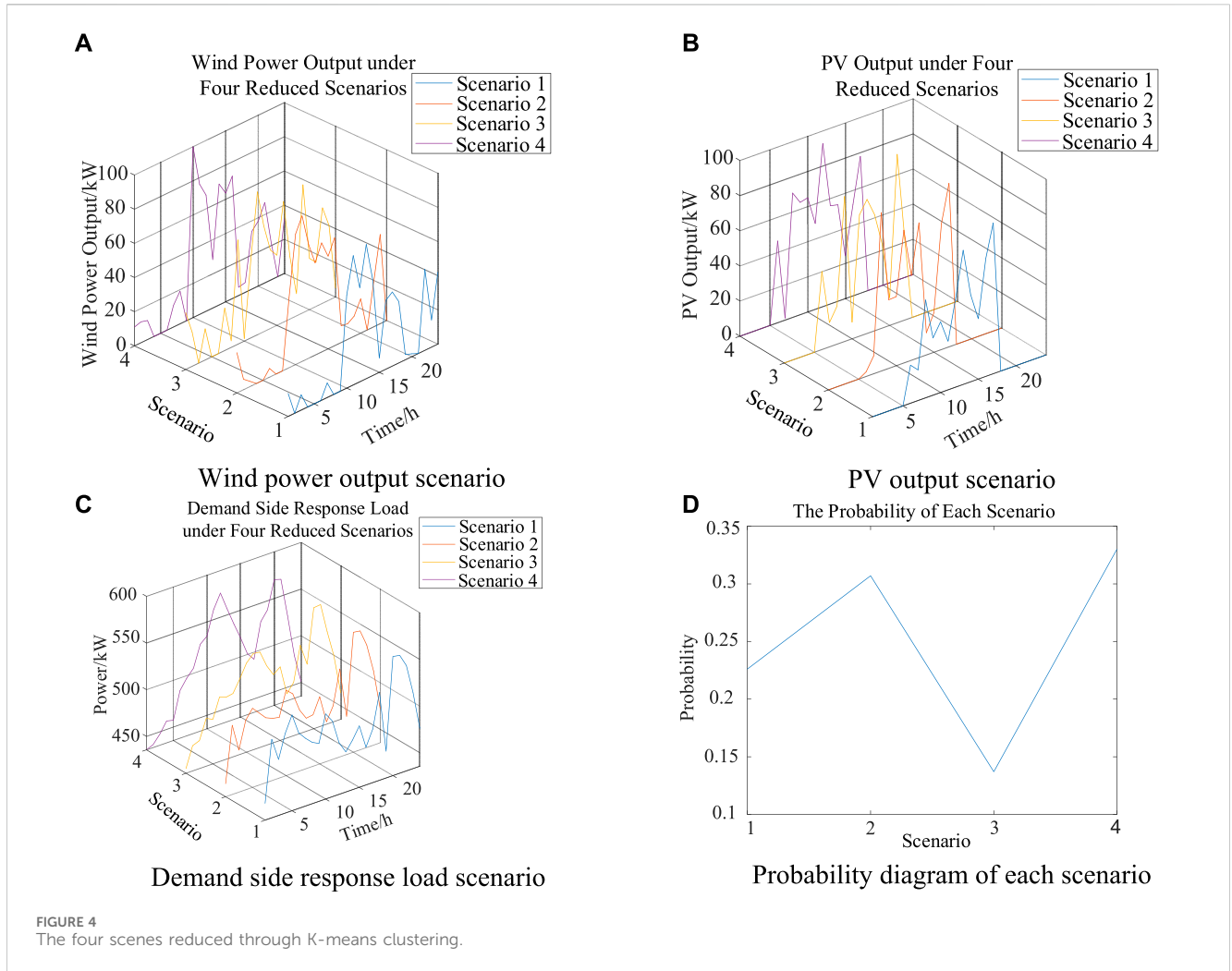Demand side response load scenario

Probability diagram of each scenario

FIGURE 4
The four scenes reduced through K-means clustering.

Where, ΔU_i represents a small increment in the voltage magnitude at node i, with a value approximately equal to 0. In most power systems, the magnitude of node voltages is approximately 1.0 per unit (pu), while the absolute value of the phase angle difference between nodes at both ends of a line rarely exceeds 30°, with most of them falling within 10° or less. Based on this scenario, the expression can be approximated as follows:

$$\begin{cases} U_i, U_j \approx 1, \quad U_i^2 \approx U_i \\ \sin\theta_{ij} \approx \theta_{ij}, \quad \cos\theta_{ij} \approx 1 \end{cases} \quad (17)$$

Thus, Eq. 15 can be further deformed, and finally the injected active power of linearized node i, as follows in Eq. 18:

$$\begin{aligned} P_{node}^i &= g_{ii}U_i + \sum_{j=1,j\neq i}^{n} g_{ij}(U_i - U_j) - \sum_{j=1,j\neq i}^{n} b_{ij}(\theta_i - \theta_j) \\ &= \left[U_i \sum_{j=1}^{n} g_{ij} + \sum_{j=1,j\neq i}^{n} (-g_{ij}U_j) \right] - \left[\theta_i \sum_{j=1}^{n} b_{ij} + \sum_{j=1,j\neq i}^{n} (-b_{ij}\theta_j) \right] \quad (18) \\ &= \sum_{j=1}^{n} G_{ij}U_j - \sum_{j=1}^{n} B_{ij}^{'}\theta_j \end{aligned}$$

Where, $B_{ij}^{'}$ excluding the self-admittance of the node. Similarly, Eq. 13 can be simplified and transformed to obtain Eq. 19. The detailed transformation process is omitted here.

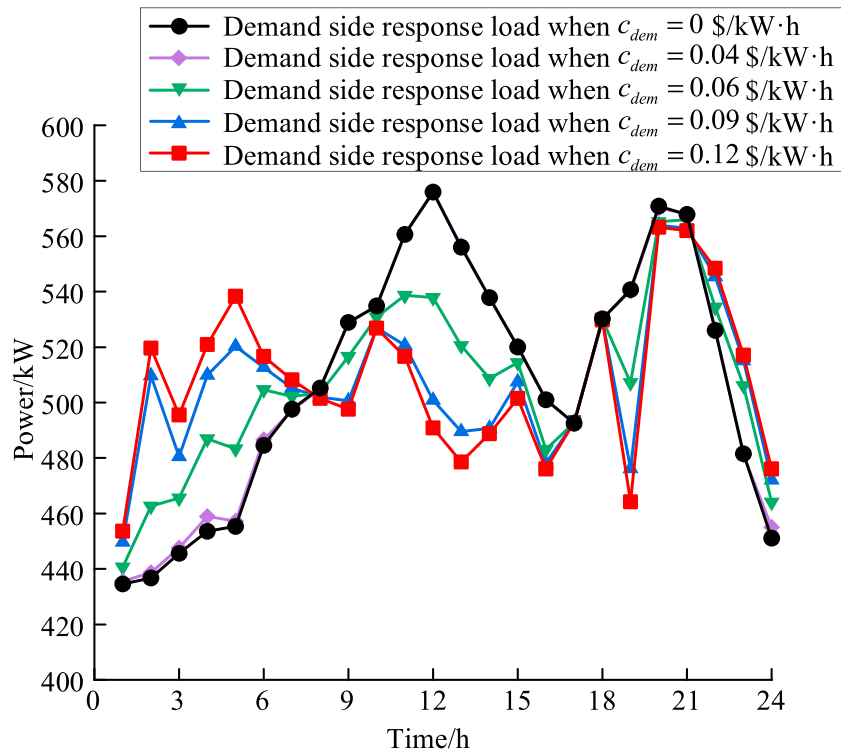$$Q_{node}^i = -\sum_{j=1}^{n} B_{ij}U_j - \sum_{j=1}^{n} G_{ij}^{'}\theta_j \quad (19)$$

FIGURE 5
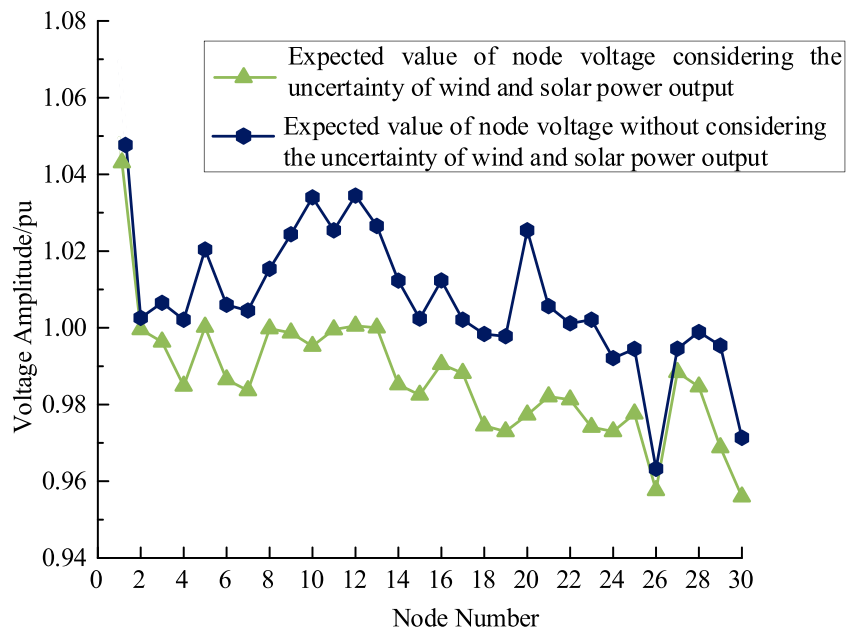Schematic diagram of demand side response effect.

FIGURE 6
Schematic diagram of expected node voltage values.

TABLE 2 The results of each model in four cases.

Model	Optimal cost/$			
	Scenario 1	Scenario 2	Scenario 3	Scenario 4
Model A	62340.987	60867.414	61175.57	63266.206
Model B	60652.546	59160.675	60048.546	61796.699
Model C	67145.944	65956.654	66115.554	67984.578
Model D	59946.549	59076.592	59491.264	60683.198
Model E	61578.254	60076.592	61019.984	62683.199

FIGURE 7
The optimal cost of each model in four scenarios.
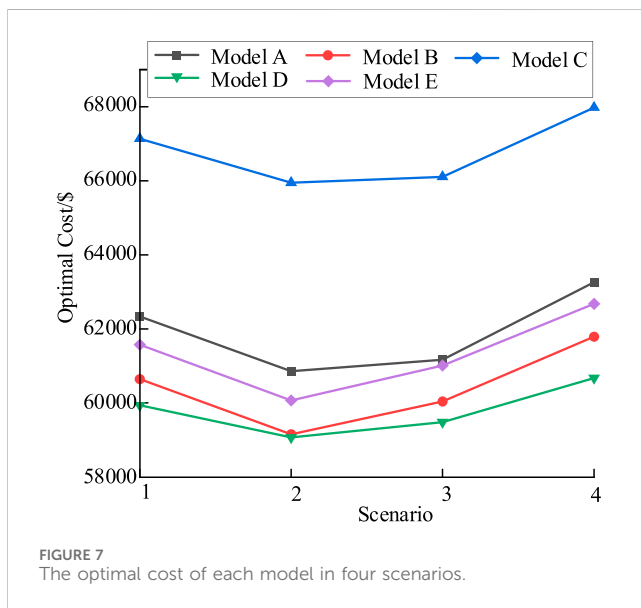
Finally, based on the calculation formula and approximate simplification of line power flow, the active power flow of line *i-j* can be derived.

After linearizing the nodal power balance equations, the OPF described in Section 4.1 was established on the MATLAB platform using the YALMIP toolbox, and solved by the commercial solver GUROBI.

5 Case study

5.1 Basis data

To validate the efficacy of the model introduced in this paper, a test was conducted on the IEEE 30-bus system. Detailed parameters for each generating unit, node, and transmission line can be found in the software package provided by MATPOWER 4.1. Two wind farms and two PV plants were integrated into the test system. The wind farms adopted constant power factor control, with an assumed power factor of 1 for all wind farms. For ease of description, the AC OPF model that accounts for the uncertainties in wind and PV power output, coupled with demand-side response, is defined as Model A. The DC OPF model considering the same uncertainties is Model B. Model C is a linear OPF model that only considers the

uncertainty of wind and PV power, while Model D focuses on the uncertainty of demand-side response. The proposed linear OPF model in this paper, which considers both wind and PV uncertainties as well as demand-side response uncertainties, is designated as Model E.

The K-means clustering method is used to reduce the generated wind power, PV and demand-side response load scenarios (Wen et al., 2023), and finally the compensated electricity price c_{dem} is 0.04 $/kW·h, 0.06 $/kW·h, 0.09 $/kW·h and 0.12 $/kW·h, respectively, as shown in Table 1 and Figure 4.

To facilitate observation and analysis, the results obtained from solving Model A are used as the benchmark and denoted as ρ_0. The specific expressions for the relative errors of the computational results from each model are detailed as follows in Eq. 20:

$$\Delta\rho = \frac{|\rho - \rho_0|}{\rho_0} \times 100\% \quad (20)$$

5.2 Case analysis

Demand-side response enables load shifting based on real-time electricity prices, avoiding usage during peak hours when electricity prices are high. This helps reduce electricity costs for users, improves economy, and serves to flatten the peak and fill the trough, thereby enhancing system stability.

By means of incorporating demand-side response and refining load curves, the resilience of the grid against uncertainties associated with renewable energy generation can be enhanced. The shifting effect of demand-side response on the load under different incentive levels is shown in Figure 5. It can be observed that as the compensation electricity price increases, the expected response quantity of users also increases, enabling a better optimization of the load curve.

As can be seen from Figure 6, the expected voltage value of the system considering the uncertainty of wind and solar power output decreases significantly. This is because the integration of wind and PV power generation can meet the active power demand of nearby nodes, thereby altering the direction and magnitude of power flow in various branches. In addition, as the output of wind and PV power generation increases, their reactive power demand also increases correspondingly, resulting in a general reduction in the voltage levels at various nodes in the system.

TABLE 3 Calculation results of five models.

Model	Optimal cost/$			Relative error/%		
	Maximum value	Minimum value	Expected value	Maximum value	Minimum value	Expected value
Model A	63266.206	60867.414	61,021.492	-	-	-
Model B	61796.699	59160.675	59604.612	2.804	2.323	2.322
Model C	67984.587	65956.654	66036.104	-	-	-
Model D	60683.198	59076.592	59,283.928	-	-	-
Model E	62683.199	60076.592	60,548.288	1.299	0.922	0.775

Table 2 and Figure 7 present the computational results of the five models under various scenarios in the test system.

As can be seen from Figure 7, a higher compensation electricity price is not necessarily better. When the compensation electricity price is between 0.09 $/kW·h and 0.12 $/kW·h, the system's scheduling cost gradually increases. Considering both the economy and uncertainty of the system scheduling cost, there exists an optimal compensation electricity price range of 0.06 $/kW·h to 0.09 $/kW·h that can result in relatively low system scheduling costs. Therefore, the average of the system dispatch costs when the compensation prices are set at 0.06 $/kW·h and 0.09 $/kW·h is taken as the expected system scheduling cost for the operator.

From Table 3, it can be observed that all five models are able to obtain optimal solutions under different scenarios, indicating that each model is feasible and effective. In various scenarios, the relative errors of Model B are all greater than 2%, with the maximum relative error approaching 3%. In contrast, the relative errors of Model E are all around 1%, representing an improvement in computational accuracy of approximately 57% compared to Model B. Therefore, the linear OPF calculation method proposed in this paper exhibits stronger applicability and can be effectively applied to online safety calculation and analysis of power systems with renewable energy sources.

Since Model C only considers the uncertainty of wind and PV outputs, its optimal cost is significantly higher than the other models. Although Model D has the lowest optimal cost, it only takes into account the uncertainty of demand-side response, which may lead to voltage and power violations, causing greater losses to the system and lacking economic feasibility. Model E has a significantly lower optimal cost than Model C, effectively reducing system operating costs. Although it is slightly higher than Model D, Model E can fully guarantee the stability and security of the system's functioning. Hence, the linear OPF model put forth in this paper, which considers the uncertainties of wind, PV and demand-side response, exhibits good economic performance while balancing system operational safety.

6 Conclusion

The OPF computation method put forth in this paper takes into account the uncertainties of wind and PV output, analyzes the uncertainty and volatility of the power system's operating state, and avoids situations where some lines of the power system are overloaded or the voltage at some nodes exceeds the limit, thereby enhancing the safety of system operation. Meanwhile, through the introduction of demand-side response, the load curve has been optimized. This significantly boosts the system's capacity to handle intermittency and unpredictability in power generation from renewable sources, further elevating the system's safety level. Additionally, it decreases the required system configuration capacity, ultimately leading to increased cost-effectiveness in the power system. The proposed method also linearizes the power flow calculations that consider multiple uncertainties, significantly reducing the computational burden and improving the calculation accuracy. This approach is more aligned with the demands of real-time safety calculation and analysis in power systems, exhibiting strong applicability and holding significant importance for online calculation and analysis of actual power systems containing uncertainty factors.

Data availability statement

The raw data supporting the conclusions of this article will be made available by the authors, without undue reservation.

Author contributions

WZ: Conceptualization, Investigation, Methodology, Software, Writing–original draft, Writing–review and editing. ZP: Conceptualization, Data curation, Formal Analysis, Methodology, Writing–review and editing. QW: Data curation, Formal Analysis, Methodology, Project administration, Validation, Writing–review and editing. WQ: Data curation, Methodology, Supervision, Writing–review and editing. YG: Formal Analysis, Funding acquisition, Project administration, Resources, Supervision, Writing–review and editing.

Funding

Conflict of interest

Publisher's note

References

Chen, G., Dong, Y., and Liang, Z. (2020). Analysis and reflection on high-quality development of new energy with Chinese characteristics in energy transition. *Proc. CSEE* 40 (17), 5493–5506.

Guo, X., Gong, R., and Bao, H. (2018). Mixed probabilistic and interval optimal power flow considering uncertain wind power and dispatchable load. *IEEJ Trans. Electr. Electron. Eng.* 13 (2), 246–252. doi:10.1002/tee.22520

Li, B., Wan, C., Li, Y., Jiang, Y., and Yu, P. (2023). Generalized linear-constrained optimal power flow for distribution networks. *IET Generation, Transm. Distribution* 17 (6), 1298–1309. doi:10.1049/gtd2.12735

Li, H., Li, H., Lu, W., Wang, Z., and Bian, J. (2020). Optimal power flow calculation considering large-scale photovoltaic generation correlation. *Front. Energy Res.* 8, 590418. doi:10.3389/fenrg.2020.590418

Li, X., Cao, J., and Du, D. (2015). Probabilistic optimal power flow for power systems considering wind uncertainty and load correlation. *Neurocomputing* 148, 240–247. doi:10.1016/j.neucom.2013.09.066

Liao, X., Xu, Y., and Wei, Z. Probabilistic power flow analysis of integrated electricity-heat energy system based on GMM and multi-point linear cumulant method Electric Power Automation Equipment, 2019, 39(08): 55–62.

Lin, Li, and Zhang, Yu (2020). *Uncertainty analysis of incentive demand response participating in optimal scheduling of active distribution network*. Jilin: Journal of North China Electric Power University 47 (5), 10–20.

Liu, Z., Wei, Z., and Gao, S. (2019). Adaptive-linearized probabilistic power flow calculation for power grid integrated with high proportion wind power in source-load interactive environment. *Power Syst. Technol.* 43 (11), 3926–3937.

Morshed, M. J., Hmida, J. B., and Fekih, A. (2018). A probabilistic multi-objective approach for power flow optimization in hybrid wind-PV-PEV systems. *Appl. Energy* 211, 1136–1149. doi:10.1016/j.apenergy.2017.11.101

Pourbehzadi, M., Niknam, T., Aghaei, J., Mokryani, G., Shafie-khah, M., and Catalão, J. P. (2019). Optimal operation of hybrid AC/DC microgrids under uncertainty of renewable energy resources: a comprehensive review. *Int. J. Electr. Power and Energy Syst.* 109, 139–159. doi:10.1016/j.ijepes.2019.01.025

Sun, Y., Wang, Y., and Wang, B. (2018). Multi-time scale decision method for source-load interaction considering demand response uncertainty. *Automation Electr. Power Syst.* 42 (02), 106–113+159.

Wen, Y., Luo, Y., Dong, X., and Xie, X. (2023). Thermal and electrical demand response based on robust optimization. *Electr. Power Syst. Res.* 225, 109883. doi:10.1016/j.epsr.2023.109883

Xie, P., Cai, Z., and Liu, P. (2019). Cooperative optimization of energy storage capacity for renewable and storage involved microgrids considering multi time scale uncertainty coupling influence. *Proc. CSEE* 39 (24), 7126–7136.

Xin, B., Shan, B., and Li, Q. (2022). Rethinking of the "three elements of energy" toward carbon peak and carbon neutrality. *Proc. CSEE* 42 (09), 3117–3126.

Yan, Y., Su, H., and Che, Y. (2018). Probabilistic power flow calculation of power system considering wind power based on improved LHS. *Acta Energiae Solaris Sin.* 39 (04), 1111–1118.

Yang, Y., Wang, Y., Gao, Y., and Gao, C. (2022). Peak shaving analysis of power demand response with dual uncertainty of unit and demand-side resources under carbon neutral target. *Energies* 15 (13), 4588. doi:10.3390/en15134588

Yang, Z., Zhong, H., Xia, Q., and Kang, C. (2018). Fundamental review of the OPF problem: challenges, solutions, and state-of-the-art algorithms. *J. Energy Eng.* 144 (1), 04017075. doi:10.1061/(asce)ey.1943-7897.0000510

Zhao, B., Wang, X., and Zhang, X. (2018). Two-layer method of microgrid optimal sizing considering demand-side response and uncertainties. *Trans. CHINA Electrotech. Soc.* 33 (14), 3284–3295.

Zhao, L., Zeng, Y., Li, Y., Peng, D., and Wang, Y. (2023). Coordinated planning of power systems under uncertain characteristics based on the multilinear Monte Carlo method. *Energies* 16 (23), 7761. doi:10.3390/en16237761

Zhao, S., Wu, Y., and Li, Z. (2022). Analysis of power system peaking capacity and economy considering the uncertainty of wind and solar output. *Power Syst. Technol.* 46 (5), 1752–1761.